Research Article

Laura Obrecht, Johannes Löw, Simon Plank, Ahmed Hadidi, Wahib Sahwan and Tobias Ullmann*

Improving flood channel detection in arid environments with Sentinel-1 InSAR coherence: a multi-sensor comparison from the April 2024 flood in Oman

https://doi.org/10.1515/geo-2025-0953
Received November 12, 2025; accepted January 14, 2026;
published online April 16, 2026

Abstract: In April 2024, northern Oman experienced an extreme flash flood triggered by rainfall totals exceeding one to two years of the regional average within 24 h. This study evaluates the performance of three remote sensing approaches for mapping flood-activated channels: Sentinel-2 Tasseled Cap Transformation (TCT) Brightness, Sentinel-1 Amplitude Change Detection (ACD), and Sentinel-1 InSAR Coherent Change Detection (CCD). Multi-temporal optical, SAR amplitude, and SAR coherence datasets were processed and compared with hydrological terrain indices derived from TanDEM-X elevation data. Results show that CCD provided the clearest and most spatially consistent delineation of flood channels, unaffected by cloud cover and less prone to noise than ACD, while integrating changes over time into a single product. Inside flow channels, coherence difference was shown to drop by up to 0.6 and being considerably lower than during stable conditions. TCT effectively highlighted bleaching of alluvial deposits under clear-sky conditions, and ACD proved most useful where flooding persisted at the time of acquisition. The combined analysis demonstrates that CCD, supported by optical and terrain data, offers a robust and transferable method for post-event flood mapping in arid regions. Its compatibility with Sentinel-1's acquisition strategies makes it a practical tool for preliminary flood mapping and post-event assessment, especially in the context of increasingly frequent extreme rainfall events.

Keywords: flashflood; InSAR coherence; sentinel-1; Oman; tasseled cap transformation; hydrologic terrain analysis

1 Introduction

From 13 to 16 April 2024, northern Oman and the United Arab Emirates experienced an unprecedented flash-flood event, with localized rainfall totals equivalent to one to two years of average precipitation, resulting in widespread infrastructure damage and significant loss of life [1]. Analyses of the event's synoptic and climatic drivers identified a rare combination of tropical–extratropical interactions as key triggers. Attribution studies further indicate that anthropogenic climate change likely intensified the rainfall [2–4]. The Arabian Peninsula is among the regions likely to experience a significant increase in future precipitation extremes [5].

In Oman, flash floods caused at least 20 fatalities, extensive damage to infrastructure, and significant disruption to daily life. Despite forecasts and early warnings, the rapid onset and magnitude of the flooding exceeded the capacity of existing flood control structures, including recharge dams. The Wadi Ahin Dam in the Wilayat of Saham in Al Batinah North Governorate suffered a breach during the event. The average rainfall in the Wadi Ahin watershed has reached 155 mm on April 16, which exceeded the storage capacity of the dam, resulting in damage to the dam spillway [6]. The event also revealed shortcomings in satellite-based

***Corresponding author: Tobias Ullmann**, Department of Remote Sensing, Julius-Maximilians University of Würzburg, 97074, Würzburg, Germany, E-mail: tobias.ullmann@uni-wuerzburg.de. https://orcid.org/0000-0002-6626-3052
Laura Obrecht, Department of Remote Sensing, Julius-Maximilians University of Würzburg, 97074, Würzburg, Germany. https://orcid.org/0009-0003-7567-3998
Johannes Löw, Department of Geoecology, Martin Luther University Halle-Wittenberg, 06120, Halle, Germany. https://orcid.org/0000-0001-8731-7534
Simon Plank, German Remote Sensing Data Center, German Aerospace Center (DLR), 82234, Wessling, Germany. https://orcid.org/0000-0002-5793-052X
Ahmed Hadidi, Department of Applied Geosciences, German University of Technology GUtech, Muscat, Sultanate of Oman. https://orcid.org/0000-0002-5349-9154
Wahib Sahwan, Leibniz Centre for Agricultural Landscape Research (ZALF), 15374, Münchberg, Germany. https://orcid.org/0000-0002-6503-5525

rainfall estimates and hydrological models, partly due to the sparse distribution of rain gauges for calibration [1].

The steep terrain, sparse vegetation and dense network of wadis make Oman particularly susceptible to flash floods. In such arid coastal catchments, intense rainfall generates high-energy runoff that converges toward outlet areas, often carrying high sediment loads from upstream erosion. These processes increase flood destructiveness and threaten agricultural areas and infrastructure [7, 8]. Mapping the activated flow channels is crucial not only for understanding sediment dynamics but also for improving flood risk management, urban planning, and flood susceptibility validation [9]. Furthermore, physical characteristics of the stream, including the length of the stream, the number of stream sub-orders, stream depth, slope degree, and the soil type are associated with the degree of damage [10].

Satellite remote sensing offers valuable tools for flood mapping, especially in regions with limited ground observations. However, optical data such as Sentinel-2 imagery are often hindered by cloud cover during flood events. Synthetic Aperture Radar (SAR), such as Sentinel-1, enables all-weather monitoring and has been widely applied for flood extent mapping using co-event backscatter changes [11, 12]. Yet, SAR intensity approaches face limitations in complex environments: urban structures create geometric distortions [13], vegetation introduces volume scattering [14], and the transient nature of flash floods often means that their surface water signal disappears before the next satellite overpass.

Interferometric SAR (InSAR) coherence offers a complementary and highly sensitive method for detecting subtle surface changes at the subpixel scale. In arid and hyper-arid regions, where vegetation is sparse, coherence loss can effectively reveal flood-induced soil disturbances and channel activation that may not be captured by SAR intensity or optical imagery. While InSAR coherence has been applied to diverse fields such as urban flood mapping [15], permafrost monitoring [16], crop phenology [17], and geomorphology [18], its potential for flash flood channel mapping in desert environments remains underexplored [8, 19–21].

This study presents a workflow for mapping flood-activated channels in selected catchments in Oman using Sentinel-1 InSAR coherence time series. We compare the derived channel network with hydrological features from TanDEM-X elevation data and optical indicators from Sentinel-2 imagery. By evaluating the performance of InSAR coherence against SAR amplitude and multispectral methods, we aim to assess its added value for understanding catchment hydrodynamics and supporting flood risk mitigation in arid environments.

2 Study area

Oman lies in an arid to hyper-arid climate zone, characterized by very low annual rainfall and strong interannual variability. Heavy rainfall events are rare, which increases uncertainty in hydrological assessments. The northern part of the country is dominated by the Hajar Mountains, extending for approximately 700 km and reaching elevations up to 3,009 m. This mountain system features steep slopes, deeply incised wadis, narrow canyons, and terraced landscapes. The geomorphology makes the region highly susceptible to flash floods when sudden, intense rainfalls occur.

Due to the arid climate, only about 2.5 % of Oman's soils are suitable for agriculture. The Batinah Plain, located along the Gulf of Oman, contains roughly half of this agricultural land. The soil is composed of calcareous sand and silt, and gravels eroded from the peridotite Hajar Mountains. Alluvial deposits in this region increase in thickness toward the coastline [22, 23]. Wadi systems typically transition from steep, confined channels in the mountains to branching alluvial channels, eventually terminating in flat alluvial plains with diffuse flow paths. These channels are dynamic, prone to shifts during high-flow events, and floodwaters often deposit thin layers of chalky material and clay on the floodplain [24, 25].

Oman exhibits a strong precipitation gradient, with annual rainfall of around 100 mm along the coast and up to 300 mm in the Hajar Mountains [26, 27]. April is typically the wettest month in the mountains, receiving an average of around 40 mm. Surface runoff is often triggered by precipitation events exceeding 5–15 mm, as rainfall is generally intense and short-lived, infiltration rates are low, and vegetation interception is minimal [25]. The impact of raindrops on bare soils can form crusts that further reduce infiltration capacity. Despite the hazard of flash floods, these rainfall events are critical for groundwater recharge, which sustains water supply in northern Oman.

In addition to seasonal rainfall, the country is exposed to tropical cyclones, particularly affecting coastal areas from Muscat to Salalah. The frequency of these events has increased from approximately two to six per decade since 1961. However, projections for future tropical cyclone activity in the region remain uncertain due to the complex interplay of climatic drivers [10, 28].

3 Methods

This study combines multi-source satellite remote sensing and terrain analysis to detect and characterize flood-

activated channels following the April 2024 flash-flood event in northern Oman. We used optical, radar, and elevation data from the Sentinel-2, Sentinel-1, and TanDEM-X missions, applying complementary processing approaches. A summary of the satellite data used is available in Table 1. (i) First, Sentinel-2 multispectral imagery was processed to detect surface changes such as bleaching effects in floodplains, using Tasseled Cap Transformation (TCT) on cloud-masked reflectance data. (ii) Second, hydrological terrain parameters – flow accumulation and the Topographic Wetness Index – were derived from the TanDEM-X 30 m Digital Elevation Model (DEM) to identify potential flow paths and water accumulation zones. (iii) Third, Sentinel-1 Ground Range Detected (GRD) data were analyzed using Amplitude Change Detection (ACD) between pre- and post-flood periods to highlight areas with significant change in radar backscatter. (iv) Finally, Sentinel-1 Single Look Complex (SLC) data were processed to generate interferometric coherence images (InSAR), allowing for Coherent Change Detection (CCD). This enables the identification of subtle flood-induced surface disturbances at the subpixel scale. CCD was based on a multi-temporal stack of Sentinel-1 SLC data, with specific pre-, co-, and post-event acquisitions selected to minimize temporal decorrelation unrelated to the flood. The integration of these methods enables a cross-comparison of optical, SAR amplitude, and InSAR coherence products for detecting flood-affected channels. The complete workflow is depicted at the end of this section in Figure 1.

3.1 Sentinel-2 analysis

Sentinel-2 data covering the study area acquired on 17 and 22 April 2024 were accessed via the Google Earth Engine (GEE) Python API, using the harmonized Sentinel-2 Surface Reflectance Collection. Cloud masks derived from the Copernicus Sentinel-2 Cloud Probability dataset were applied in a subsequent step. To enhance the visibility of flood-induced surface changes, particularly bleaching in alluvial plains, we applied TCT using coefficients for the six Sentinel-2 MSI bands [29]. The resulting indices (i.e., Tasseled Cap Brightness) were visually inspected to identify areas affected by the April 2024 flash flood.

Table 1: Satellite datasets used in this study and the associated analysis performed.

Dataset	Analysis	Acquisition date
Sentinel-2 MSI	TCT brightness	17, 22 April 2024
Sentinel-1 GRD	ACD	26 March, 19 April 2024
Sentinel-1 SLC	CCD	26 March, 7, 19 April 2024
TanDEM-X 30 m EDEM	TWI, flow accumulation	–

3.2 Hydrological terrain analysis

Hydrological parameters were calculated from four TanDEM-X 30 m Edited DEM (EDEM) tiles covering the study area, obtained from the DLR Geoservice Platform. The tiles were mosaicked, reprojected to the study's coordinate reference system, and processed in SAGA GIS 9.7.1 to derive Flow Accumulation and the Topographic Wetness Index (TWI) employing standard toolchains [30]. These layers provide topographic estimates on potential flood pathways and support the interpretation of both optical and radar-derived change maps. Earlier research has pinpointed TWI, along with other terrain indices, as a useful tool in identifying regions in Oman that are susceptible to flash flooding [9].

3.3 Sentinel-1 amplitude change detection (ACD)

Sentinel-1 GRD imagery was processed in GEE using the pre-processed S1_GRD collection, which includes thermal noise removal, radiometric calibration, and terrain correction. Two mosaics of VV-polarized backscatter were generated: one pre-flood (26 March 2024) and one post-flood (19 April 2024). ACD was calculated by subtracting the pre-flood mosaic from the post-flood mosaic, highlighting areas with significant changes in surface backscatter attributable to flooding.

3.4 Sentinel-1 InSAR coherence change detection (CCD)

A total of 40 Sentinel-1 VV/VH Single Look Complex (SLC) scenes (relative orbit 57) were downloaded from the Alaska Satellite Facility. Unlike GRD products, SLC data preserve both amplitude and phase information, enabling interferometric analysis. The study area is covered by two SLC tiles, that were processed using a hybrid workflow combining the pyroSAR PythonAPI [31] and the Sentinel Application Platform (SNAP) [32], integrated within an Open Data Cube environment for streamlined data management [33]. The scenes were debursted with the S1 TOPSAR Deburst in SNAP. Interferometric coherence processing included multi-looking (1 azimuth $\times$ 4 range looks) and Range-Doppler Terrain Correction. For the coherence estimation, flat-earth

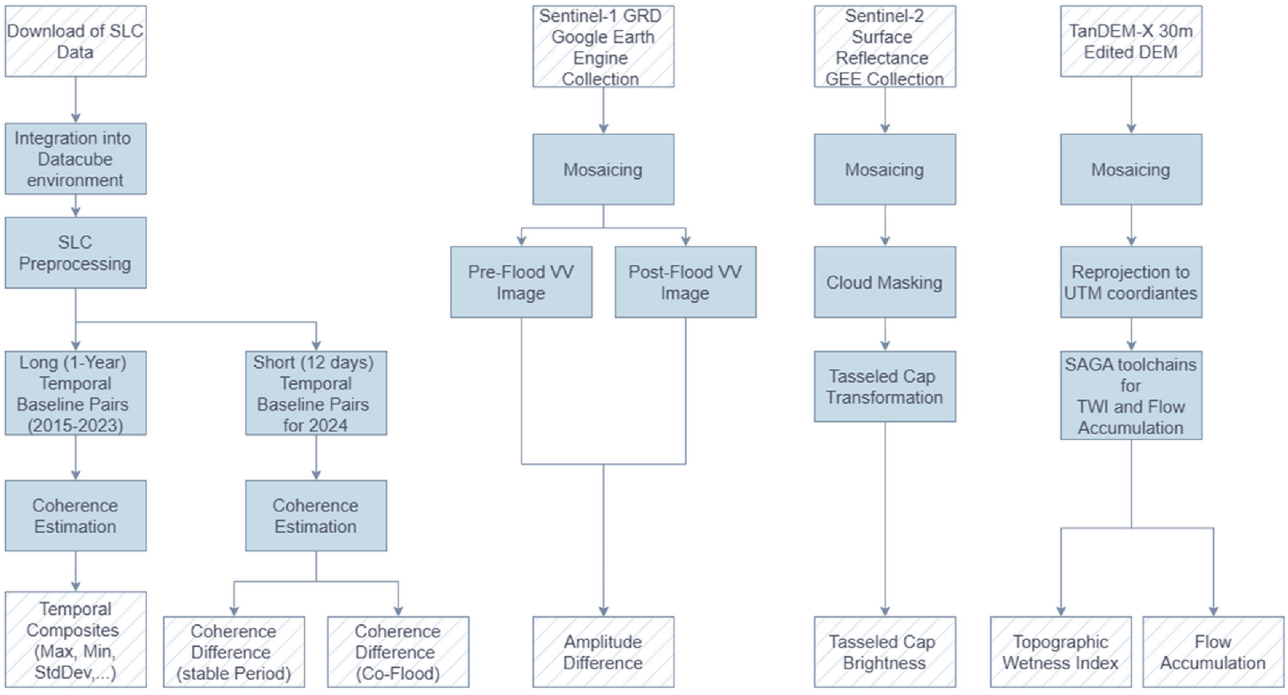

Figure 1: Flowchart showing data processing steps from Sentinel imagery and DEM to flood mapping.

and topographic phase removal was incorporated using a 3 × 11 pixel moving window (azimuth × range) producing coherence at a 20 m pixel spacing [16].

We initially applied two complementary coherence-based processing strategies to exploit the full Sentinel-1 SLC archive for the study area. (i) To characterize the natural spatio-temporal variability of interferometric coherence and to identify surfaces with persistently low coherence (e.g., sand, dense vegetation, radar shadows), we processed one VV-polarized SLC acquisition per November from 2015 to 2023. These acquisitions, each separated by approximately one year, were combined into interferometric pairs with long temporal baselines. Coherence images were generated following the workflow described in [34]. From the stack of long temporal baseline coherences (pairs 2015/2016, 2016/2017, …) temporal features (minimum, maximum, mean, median, standard deviation, quartiles) were derived for each pixel. This long-term coherence stack serves as a reference for interpreting short-term changes during the April 2024 flood. (ii) To isolate and analyse flood-induced surface changes, we used a short (12 days) temporal baseline approach centred on the 15 April 2024 flooding. Three Sentinel-1 VV/VH acquisitions were selected: pre-event (t_1 = 26 March 2024), intermediate/pre-flood (t_2 = 7 April 2024), and post-event (t_3 = 19 April 2024). Interferometric coherence was calculated for the pre-disaster pair (t_1/t_2) and the co-/post-disaster pair (t_2/t_3). The coherence values of an image pair reach from 0 (low coherence) to 1 (high coherence). The coherence difference was computed as:

$$\text{Coherence Difference} = \text{COH}(t_2, t_3) - \text{COH}(t_1, t_2)$$

The short temporal baselines minimize decorrelation unrelated to the flooding, increasing sensitivity to fluvial activity and sediment redistribution. Although we initially tested masking known low-coherence areas from the long-term analysis (i), we ultimately based the main analysis on the direct pre-post event coherence difference, which yielded a clear and interpretable depiction of flood-induced surface changes. This simplified approach ensured that no flood-related surface changes would be overlooked by masking parts of the image. As a reference, we compared the coherence difference image of the event to the coherence difference during a flood-free period (t_1 = 2 January, t_2 = 14 January and t_3 = 26 January 2024).

To quantitatively assess the robustness of the CCD-based mapping, we conducted a threshold sensitivity analysis for the coherence difference and TCT brightness values. For both approaches, a range of thresholds was systematically applied, and the resulting mapped area was expressed as a fraction of the total analysis domain. This allowed direct comparison of how sensitive each method is to threshold selection. Threshold-area fraction relationships were then plotted for coherence difference and TCT brightness to

evaluate internal consistency and relative stability across the tested parameter space.

4 Results

The results are presented in four steps: (i) Sentinel-2-based TCT, (ii) Sentinel-1 backscatter analysis via ACD, (iii) Sentinel-1 InSAR CCD, and (iv) combined interpretation with hydrological terrain metrics.

4.1 Sentinel-2 analysis

Figure 2 shows the TCT Brightness for mosaics acquired on 17 April (left) and 22 April 2024 (right). Despite extensive cloud cover on 17 April, numerous runoff channels are visible in green–orange tones, indicating elevated brightness relative to the surrounding terrain. The inset in the lower left highlights the breach of the Wadi Ahin Dam (cf. Section 1), where fine green flow channels contrast against the low-brightness background. In the eastern portion of the study area, imaged on 22 April, water had largely drained, but the flood-affected areas exhibit higher brightness values than before, with major bleaching visible in orange to red. The inset in the upper right shows the Wadi Maawil and Wadi Bani Kharous catchments, where flow channels feeding into the dam are clearly identifiable. Unimpeded water to the left of the dam reached inhabited coastal zones.

4.2 Sentinel-1 amplitude change detection

The Sentinel-1 ACD results (Figure 3) display the difference between post-flood (15/22 April) and pre-flood (17/29 March) VV backscatter. Most areas show minimal change (white to pale red/blue and values around 0), but distinct amplitude anomalies are visible in selected locations. The dam breach (cf. Section 1) is evident in the lower-left inset: the reservoir

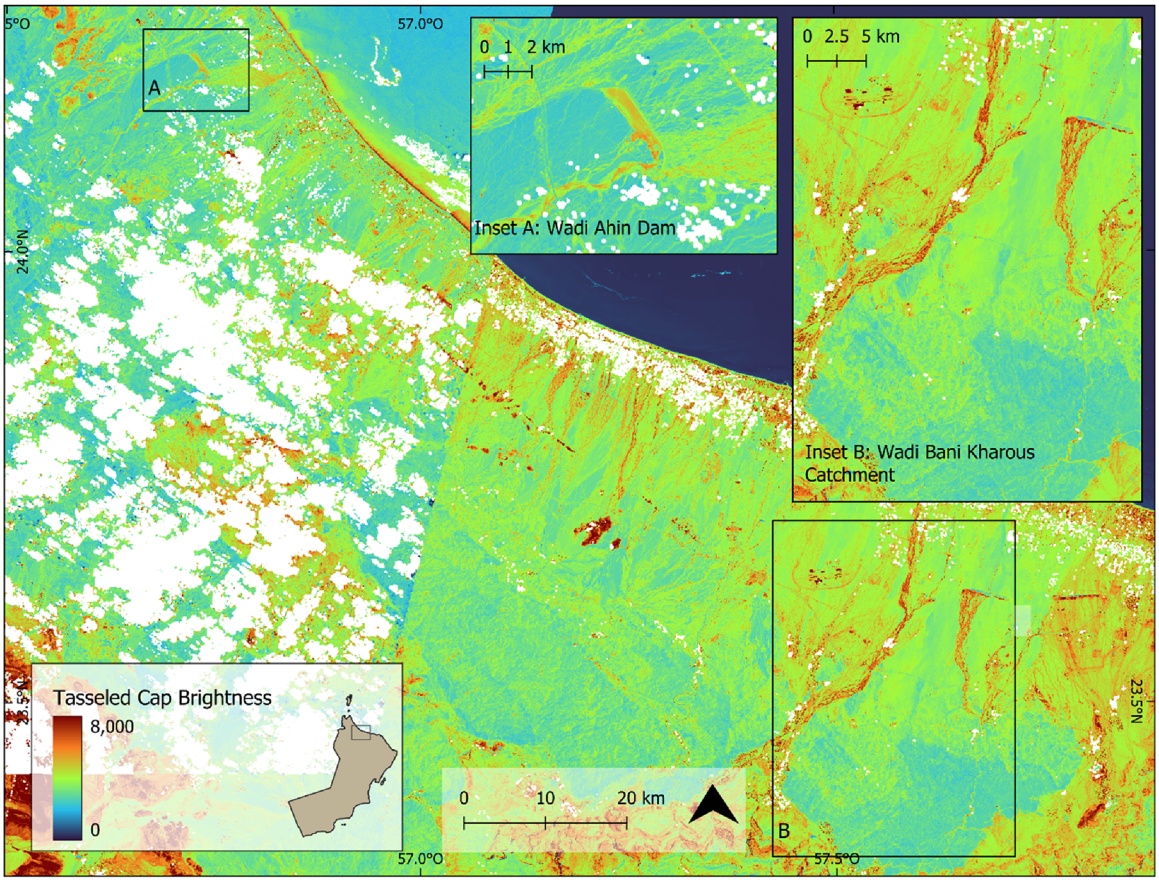

Figure 2: Map highlighting flooded areas in green/orange using Sentinel-2 brightness data post-flood.

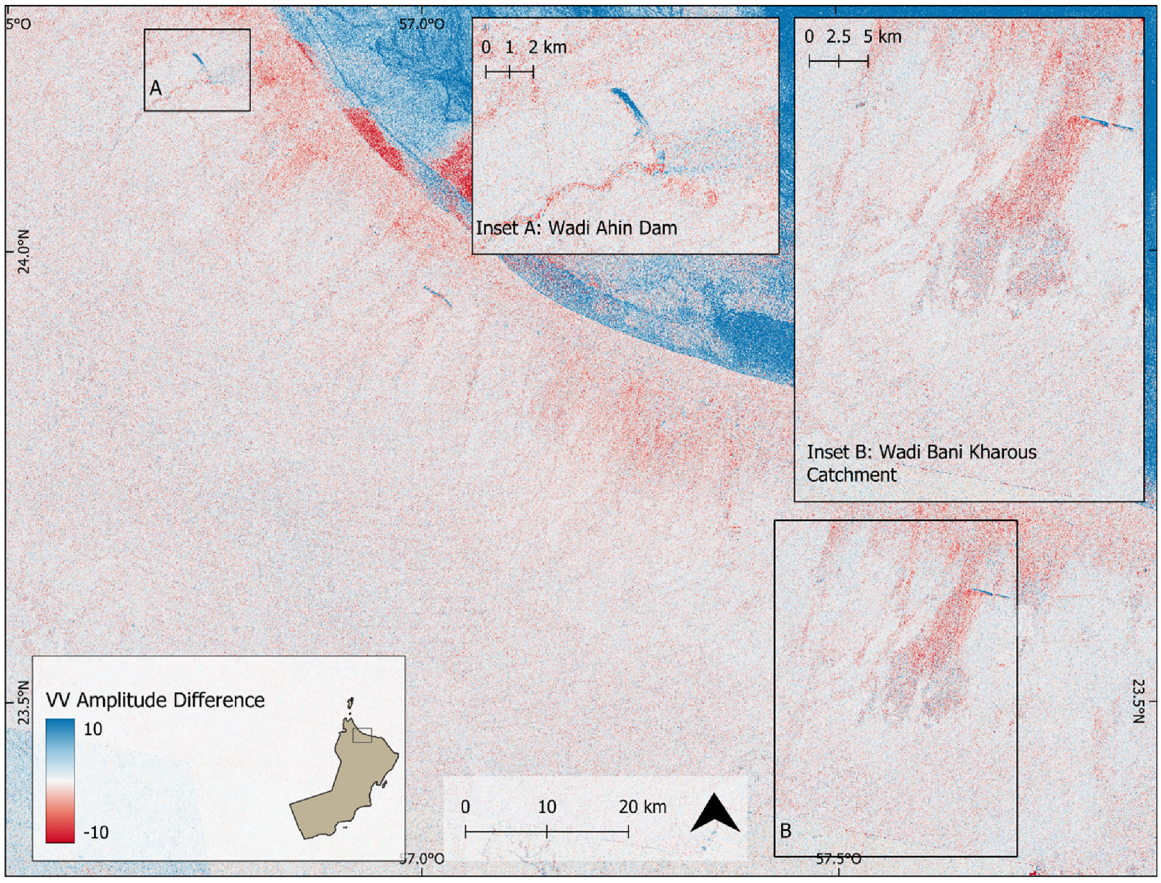

Figure 3: Map showing flood extent in blue and red from Sentinel-1 amplitude change pre/post-flood.

area shows a positive amplitude change, while the upstream channel has a negative change. Coastal dams appear in blue, reflecting lower post-flood backscatter from open water. Some flow channels are faintly visible as light-red streaks, especially along the coastline. In the Wadi Bani Kharus catchment, stronger negative changes occur in the alluvial fan area, but the complex backscatter pattern hampers clear channel delineation, unlike in the Sentinel-2 TCT imagery.

4.3 Sentinel-1 InSAR coherence change detection

Figure 4 presents the CCD results derived from short-baseline interferometric pairs (26 March/7 April and 7 April/19 April 2024). Negative coherence differences (red) indicate flood-induced surface disturbance, whereas positive values (blue) occur along mountain slopes (most likely) due to geometric effects and radar shadowing. A fine network of high negative coherence difference flow channels extends along the entire coastline, connecting mountain slopes to inhabited downstream areas. The strongest losses in coherence (up to −0.95) occur near the dam breach, while smaller channels exhibit more moderate decreases (around −0.5 to −0.8). Compared with coherence differences during a stable period (Figure 5), flood-time values are evident and clearly visible. At approximately 5 km from the coast, the clear signal of the coherence difference is obscured, as the landscape is dominated by agricultural fields and settlements. This phenomenon is also evident during the stable period (see Figure 5), where the difference is approximately zero on the plains, in contrast to the coastline, where no distinct signal can be discerned.

4.4 Combined hydrological analysis

The Topographic Wetness Index (TWI) derived from the TanDEM-X DEM (Figure 6) highlights the terrain's likelihood

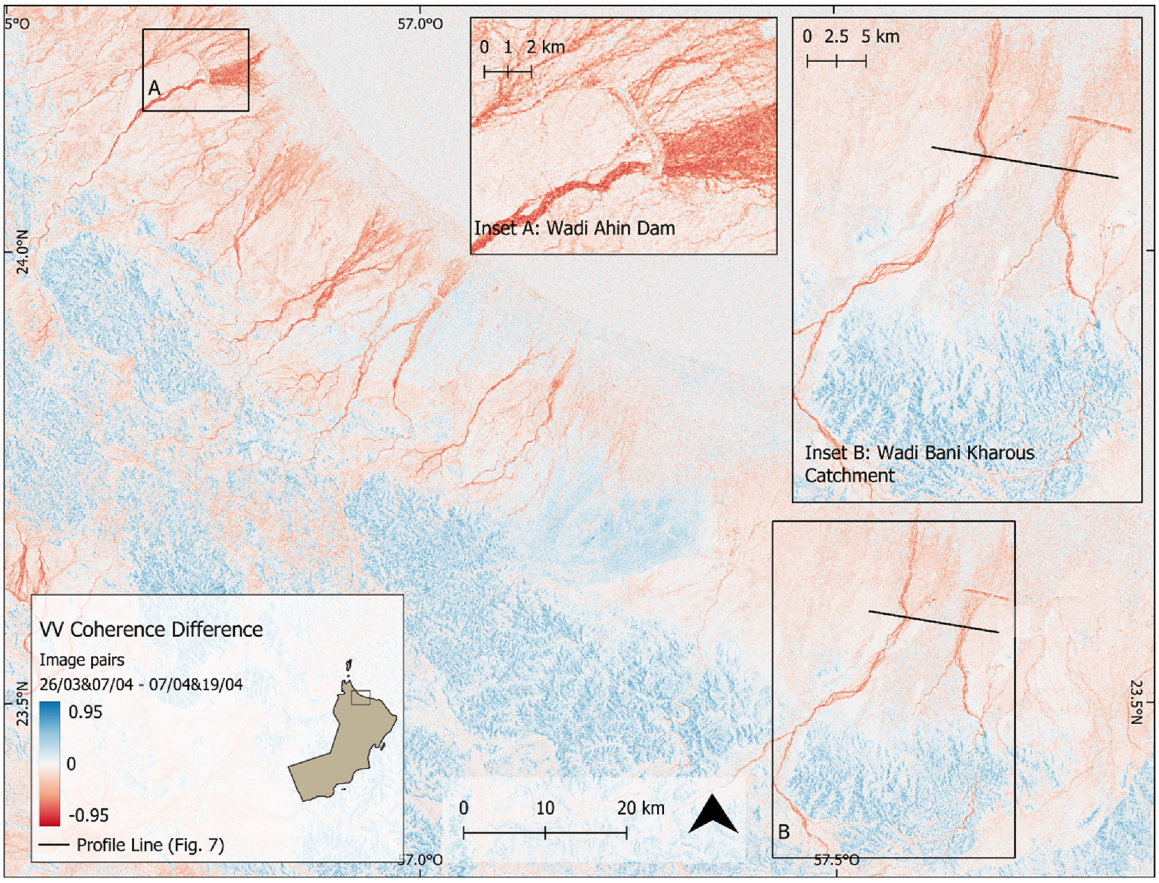

Figure 4: Map of coherence loss in red indicating flooded areas post-event.

to accumulate water. Low TWI values (orange) dominate steep mountain areas, while higher values (blue) occur in the coastal plain. Key flood channels identified in Sentinel-2 and Sentinel-1 analyses align closely with high-TWI corridors. Notably, the dark-blue channel in the lower left map corresponds to the dam-breach path seen in the CCD (Figure 4) and TCT (Figure 2) images. Similarly, in the Wadi Maawil and Bani Kharous catchment, high-TWI channels match the main flood pathways. Figure 6 shows a cross-section of the two catchments, as located in Figure 4: during the flood (black), coherence drops sharply at x = 4,000 and x = 12,000, coinciding with peaks in TCT Brightness (green). In Figure 4, these sharp drops can be recognised as flow channels crossing the cross-section vertically. The co-event coherence difference is up to 0.6 lower than during the stable conditions. Stable-period differences (grey) remain within the range of the coherence difference standard deviation for the entire cross-section, while the flood-affected coherence difference is significantly lower for the entire profile, symbolized by the red fill between the coherence profiles. Only a limited number of components of the profile are colored blue, thereby signifying that the stable coherence is found to be lower than the flood-affected coherence. As illustrated in Figure 7, high Flow Accumulation values (>10^6, represented by blue bars) correspond to the drops in coherence and peaks in TCT Brightness. This is especially evident for the coherence drop at x = 4,000.

Both CCD and TCT exhibit a similar relationship between threshold value and mapped area fraction, visual in Figure 8. At low thresholds, large portions of the study area are classified, followed by a transitional regime characterized by a rapid change in area fraction over a narrow threshold range. At higher thresholds, the curves approach minimal mapped areas, indicating increasingly conservative classification. This suggests comparable sensitivity behaviour between CCD and TCT.

5 Discussion

This study evaluated the suitability of optical, SAR amplitude, SAR coherence, and terrain-based products for

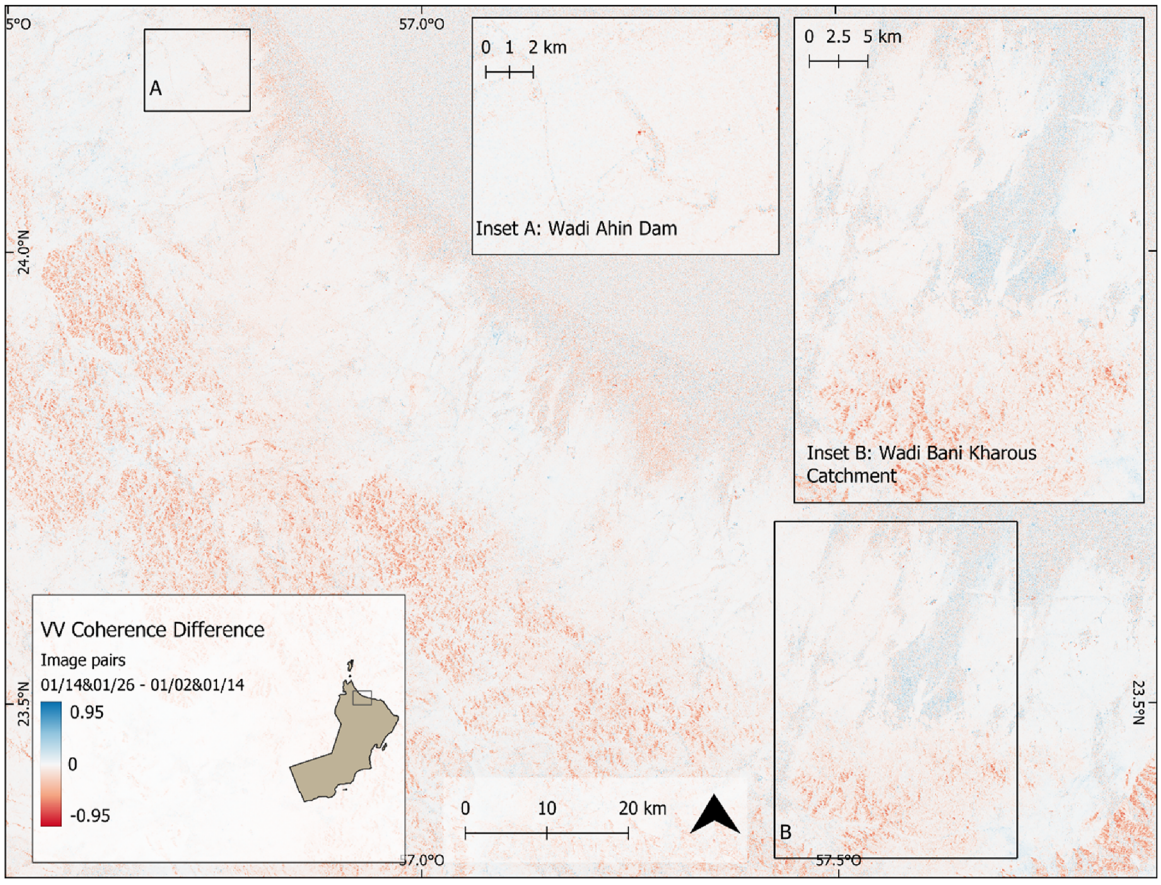

Figure 5: Map showing stable coherence values across landscape during non-flood period.

mapping flood-activated channels after the April 2024 flash flood in northern Oman. Each data source exhibited distinct strengths and limitations. The Tasseled Cap Transformation (TCT) applied to Sentinel-2 imagery successfully highlighted flood-affected surfaces, with the bleaching of alluvial deposits emerging as a particularly effective indicator for channel mapping. This bleaching effect was especially valuable for differentiating active flow paths from surrounding terrain and is consistent with findings by [18], who demonstrated similar utility of post-flood spectral changes in arid regions. However, TCT's operational use was constrained by extensive cloud cover during the event, which limits its suitability for systematic or near-real-time monitoring. Under clear-sky conditions, it remains a powerful supplementary dataset for interpreting SAR-derived products and validating flood extent maps.

Amplitude Change Detection (ACD) from Sentinel-1 GRD data, unaffected by cloud cover, produced comparatively noisy outputs, which complicated the clear delineation of channels. Nevertheless, the method is particularly well-suited for regions where flooding is still present at the time of satellite overpass, as standing water produces distinct backscatter signatures that enhance detectability [11]. Given its rapid computation and minimal pre-processing requirements, ACD remains a practical first-look product for emergency response, even if its accuracy is lower than that of more advanced methods.

Coherence Change Detection (CCD) from Sentinel-1 SLC data provided the clearest and most consistent delineation of flood-activated channels. Its main strength lies in integrating changes over time into a single product, capturing both immediate and short-term post-flood disturbances. This temporal integration not only creates a comprehensive picture of the flood impact but also offers potential advantages for validating hydrological and hydraulic models, where cumulative channel activation patterns are important for model calibration. Like ACD, CCD requires pre- and post-event acquisitions, which can delay product availability, but being unaffected by clouds and well interpretable, makes it an invaluable tool for post-event

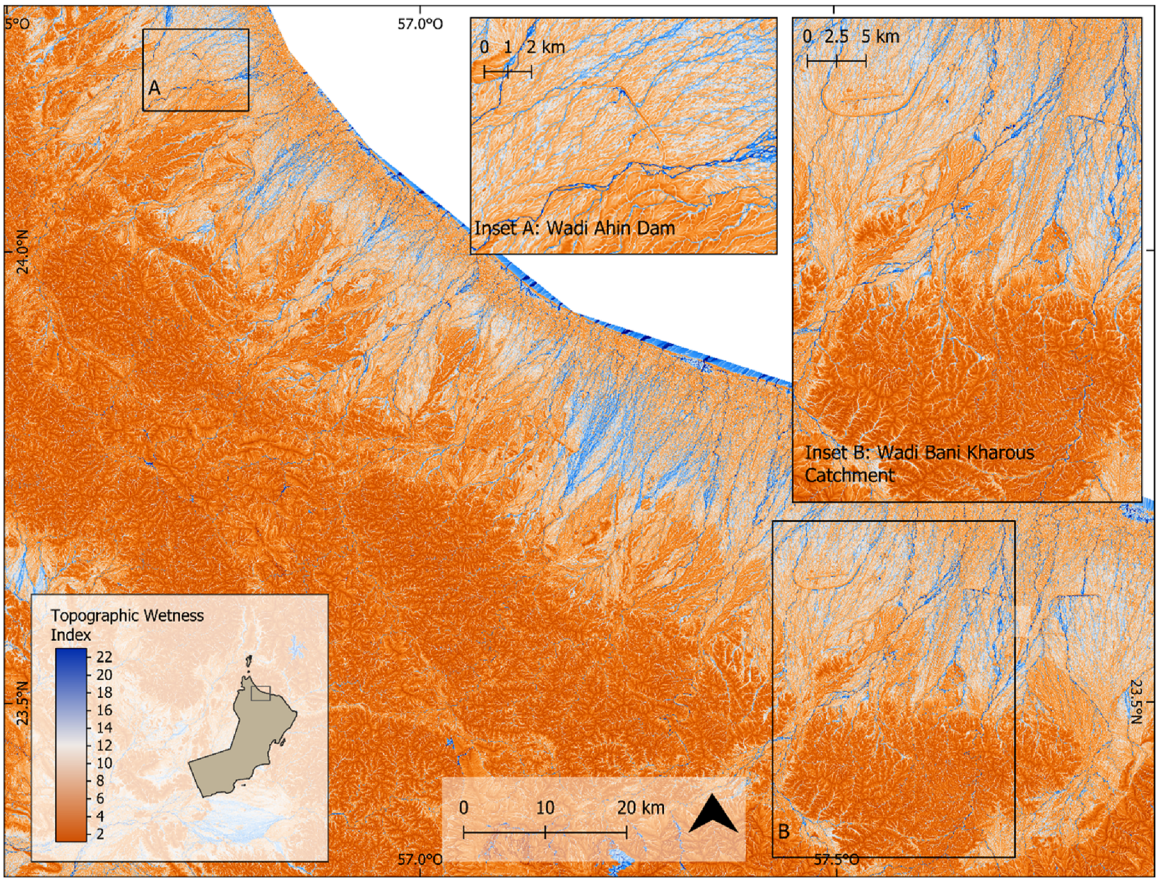

Figure 6: Map of wetness potential with high values in blue along rivers and wadis.

analysis. The main limitations of CCD occur in areas with complex topography, where geometric distortions can obscure change signals, and in landscapes that do not produce a stable, coherent return, such as dense vegetation or shifting sand. In coastal agricultural zones, rapid and frequent land-management activities generate strong decorrelation signals that are not related to hydrologic forcing, making it difficult to uniquely attribute coherence loss to flash-flood processes [17, 35]. Studies of CCD consistently note that vegetation cover is a primary limitation, as coherence may already be low during stable conditions, making it difficult to distinguish between hydrologic disturbance and normal canopy dynamics. On the other hand, in dense urban fabrics, CCD can be oversensitive: many non-hazard related changes cause decorrelation. Studies that map floods in urban environments with coherence require a more complex workflow, including *a priori* information on urban masks to generate a stable prediction of flood pathways [36].

For this reason, the combined use of long-temporal baseline data to characterize background coherence and short-temporal baseline data to detect event-related changes is recommended. Still, the distinct drop in coherence following the April 2024 flash flood made these additional steps unnecessary. This highlights both the robustness of short-baseline CCD in arid environments and the situational role of long-term coherence statistics. In regions with denser vegetation, such composites remain an important methodological complement for distinguishing true surface changes from natural variability.

Hydrological terrain analysis based on the Flow Accumulation and the Topographic Wetness Index (TWI), derived from the TanDEM-X DEM, proved most useful as a baseline for assessing the correspondence between predicted and observed flow pathways. However, there are important limitations: extreme flood events of the magnitude observed in April 2024 can alter channel morphology, meaning that the DEM may not fully represent the current terrain

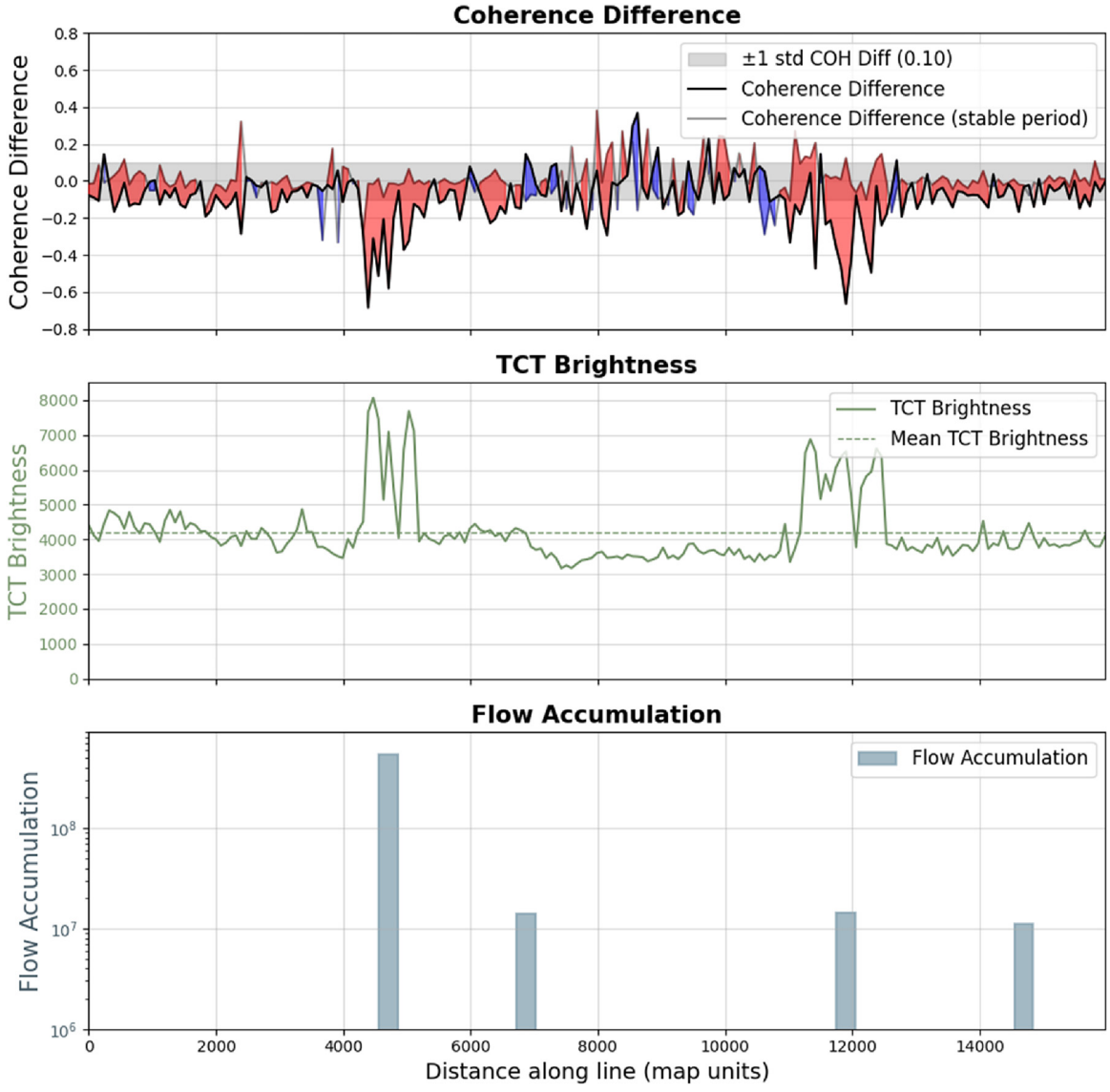

Figure 7: Three line plots comparing coherence drop, brightness increase, and flow accumulation along flood channel profile.

configuration. Flash floods in arid basins can rapidly incise channels, rework bars and avulse across alluvial fans, producing significant morphological change in a single event [37]. Furthermore, the 30 m spatial resolution is insufficient for detecting small-scale flow paths. Future applications could benefit from higher-resolution and regularly updated elevation datasets, such as those generated from very high-resolution optical stereo and airborne LiDAR, which would allow for more precise modeling of flood pathways, albeit at a higher acquisition cost [9]. The DEM acquisition predates major flood events by several years, so the TanDEM-X 30 m represents pre-event morphology, while post-event channels may diverge substantially, making TWI and flow accumulation maps increasingly misaligned with observed channel paths. Integrating DEM-derived morphometrics with event-based observations allow for identification of where DEM-based channel predictions remain robust and where morphological updating is required [38].

The SAR-based approaches tested here are transferable to any region with adequate Sentinel-1 coverage, typically a 12-day repeat cycle, provided that high-quality DEMs are available to reduce topographic artifacts in mountainous areas. CCD was particularly effective in arid and hyper-arid regions with sparse vegetation cover, where volume scattering is

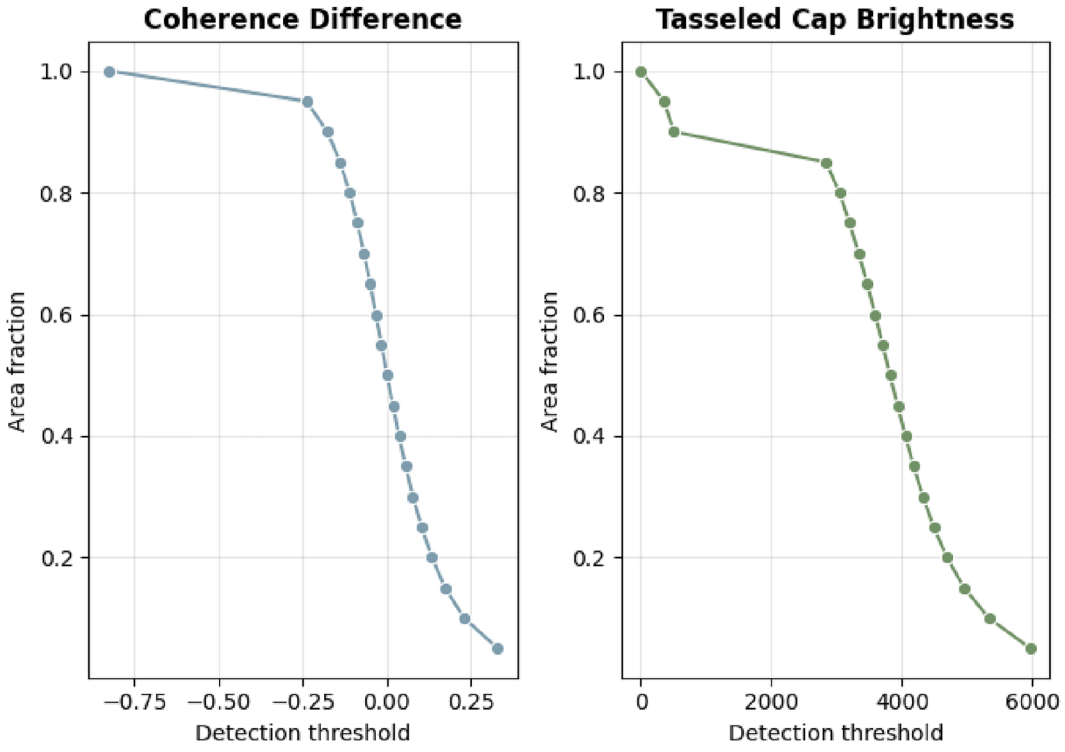

Figure 8: Scatterplot comparing coherence and brightness thresholds against area fraction, showing linear relationship.

minimal. In northern Oman, however, tracing channels through vegetated coastal zones proved challenging due to decorrelation caused by scattering from plant canopies. Similar limitations are expected in more humid, densely vegetated regions, where L-band data, from e.g., the ALOS-2/4 and the recently launched NISAR mission, should be used due to their higher long-term coherence. Conversely, previous studies have shown strong potential for C-band CCD in urban environments, where stable man-made surfaces preserve coherence well [39].

Our findings are consistent with earlier research demonstrating the sensitivity of InSAR coherence to flood-induced surface changes in arid landscapes, such as in Libya, where CCD combined with Principal Component Analysis was used to map erosion features after flash floods [8]. Another study in the Draâ Valley in southern Morocco showed that coherence loss could be attributed to sediment transport due to flash floods [21]. Comparable workflows have also been applied in landslide detection [40], highlighting the broader applicability of CCD for rapid geomorphological change mapping. Recent developments in multi-temporal InSAR and coherence modeling for disaster monitoring may further improve flood channel mapping, especially when integrated with multi-sensor datasets [41].

While the sensitivity analysis does not replace independent ground validation, it offers a pragmatic internal benchmarking approach in data-scarce environments. Future work could combine this analysis with targeted field observations or very-high-resolution post-event imagery to better constrain the optimal threshold range and assess classification accuracy at feature-level scales such as channel width or deposit margins.

For Oman, the capacity to rapidly and accurately map flood-activated channels has direct implications for disaster readiness, infrastructure design, and water resource management. Detailed channel mapping can identify recurring flood pathways for targeted reinforcement of dams, embankments, and drainage infrastructure. It also enables post-event evaluations of dam performance and highlights areas where hydraulic capacity was exceeded. Such information can inform urban planning in coastal plains, helping to avoid settlement expansion into high-risk corridors [42]. Furthermore, accurate channel mapping can enhance the calibration and validation of hydrological models underpinning early warning systems. Considering the increasing likelihood of extreme precipitation events under climate change, integrating CCD into operational disaster management frameworks could significantly strengthen Oman's resilience to flash floods [43].

6 Conclusions

In April 2024, northern Oman experienced an exceptional flash flood triggered by rainfall exceeding one to two years of the regional average precipitation within 24 h. This study assessed the performance of Sentinel-2 Tasseled Cap Transformation (TCT) Brightness, Sentinel-1 Amplitude Change Detection (ACD), and Sentinel-1 InSAR Coherent Chance Detection (CCD) for mapping the resulting flood-activated channels. Among these, CCD produced the clearest and most spatially consistent results, unaffected by cloud cover and less prone to noise than ACD, while its temporal integration of surface changes provided a more complete picture of flood impacts. TCT offered valuable supplementary information under clear-sky conditions, and ACD proved most effective where standing water persisted at the time of acquisition. The findings highlight CCD's strong potential for application in arid and hyper-arid regions, where sparse vegetation supports high coherence stability. Its compatibility with Sentinel-1's acquisition strategies makes it a practical tool for preliminary flood mapping and post-event assessment, especially in the context of increasingly frequent extreme rainfall events.

Acknowledgments: We acknowledge the European Space Agency for providing free access to Sentinel-1 and Sentinel-2 data, and the Google Earth Engine for offering cloud-based processing capabilities. We also thank the Alaska Satellite Facility for access to Sentinel-1 SLC data. The TanDEM-X 30 m Edited DEM tiles were kindly provided by the German Aerospace Center (DLR) through its Geoservice platform.

Author contributions: Conceptualization, L.O. and T.U.; methodology, L.O.; software, L.O., J.L.; validation, L.O.; formal analysis, L.O.; investigation, L.O.; resources, T.U.; writing – original draft preparation, L.O., J.L.; writing – review and editing, L.O., J.L., S.P., A.H., T.U., W.S.; visualization, L.O.; supervision, T.U. All authors have read and agreed to the submitted version of the manuscript.

Conflicts of interest: The authors declare no conflict of interest.

Funding statement: This work received no external funding.

References

1. Hussein K, Alhosani N, Al-Areeq AM, Al Aghbari AA, Elkamali M, Alsumaiti T, et al. Unprecedented rainfall in the United Arab Emirates: hydrologic and flood impact analysis of the April 2024 event. Nat Hazards 2025;121:9363–85.
2. Francis D, Fonseca R, Nelli N, Cherif, C, Yarragunta, Y, Zittis, G, et al. From cause to consequence: examining the historic April 2024 rainstorm in the United Arab Emirates through the lens of climate change. npj Clim Atmos Sci 2025;8:183.
3. Latif M, Usman M, Malik A, Masabathini S, Ahmad B, Atique L, et al. Tropical-extratropical interactions: the atmospheric dynamics behind Dubai's extreme precipitation in April 2024. Nat Hazards 2025;121: 19017–47.
4. Zachariah M, Kimutai J, Barnes C, Gryspeerdt E, Seneviratne S. Heavy precipitation hitting vulnerable communities in the UAE and Oman becoming an increasing threat as the climate warms. World Weather Attribution 2024. https://doi.org/10.25561/110910.
5. Gründemann GJ, van de Giesen N, Brunner L, van der Ent R. Rarest rainfall events will see the greatest relative increase in magnitude under future climate change. Commun Earth Environ 2022; 3:235.
6. Kothaneth L. MoAFWR officials monitor dams. Oman Dly Obs [Internet] 2024. Available from: https://www.omanobserver.om/article/1152745/oman/moafwr-officials-monitor-dams.
7. Marchi L, Borga M, Preciso E, Gaume E. Characterisation of selected extreme flash floods in Europe and implications for flood risk management. J Hydrol 2010;394:118–33.
8. Normand JCL, Heggy E. Assessing flash flood erosion following storm daniel in Libya. Nat Commun 2024;15:6493.
9. Al-Kindi KM, Alabri Z. Investigating the role of the key conditioning factors in flood susceptibility mapping through machine learning approaches. Earth Syst Environ 2024;8:63–81.
10. Al-Awadhi T, Abdullah M, Al-Ali Z, Abulibdeh A, Al-Barwani M, Al Nasiri N, et al. Navigating cyclone threats: a forecast approach using water streams' physical characteristics as an indicator to predict high risk potential areas in the Sultanate of Oman. Earth Syst Environ 2024; 8:937–49.
11. Twele A, Cao W, Plank S, Martinis S. Sentinel-1-based flood mapping: a fully automated processing chain. Int J Rem Sens 2016;37: 2990–3004.
12. Bereczky M, Wieland M, Krullikowski C, Martinis S, Plank S. Sentinel-1-Based water and flood mapping: benchmarking convolutional neural networks against an operational rule-based processing chain. IEEE J Sel Top Appl Earth Observations Remote Sensing 2022; 15:2023–36.
13. Samuele DP, Filippo S, Orusa T, Enrico BM. Mapping SAR geometric distortions and their stability a long time: a new tool in google Earth engine based on Sentinel-1 image time series. Int J Rem Sens 2021;42: 9135–54.
14. Plank S, Jüssi M, Martinis S, Twele A. Mapping of flooded vegetation by means of polarimetric Sentinel-1 and ALOS-2/PALSAR-2 imagery. Int J Rem Sens 2017;38:3831–50.
15. Pulvirenti L, Chini M, Pierdicca N, Boni G. Use of SAR data for detecting floodwater in urban and agricultural areas: the role of the interferometric coherence. IEEE trans. Geosci. Remote Sens 2016;54: 1532–44.
16. Zhang Z, Wang C, Zhang H, Tang Y, Liu X. Analysis of permafrost region coherence variation in the Qinghai–Tibet Plateau with a high-resolution TerraSAR-X image. Remote Sens 2018;10:298.
17. Löw J, Ullmann T, Conrad C. The impact of phenological developments on interferometric and polarimetric crop signatures derived from Sentinel-1: examples from the DEMMIN study site (germany). Remote Sens 2021;13:2951.
18. Ullmann T, Sauerbrey J, Hoffmeister D, May SM, Baumhauer R, Bubenzer O, et al. Assessing spatiotemporal variations of Sentinel-1 InSAR coherence at different time scales over the atacama desert (chile) between 2015 and 2018. Remote Sens 2019;11:2960.

19. Amitrano D, Di Martino G, Di Simone A, Imperatore P. Flood detection with SAR: a review of techniques and datasets. Remote Sens 2024;16: 656.
20. Chaabani C, Chini M, Abdelfattah R, Hostache R, Chokmani K. Flood mapping in a complex environment using bistatic TanDEM-X/TerraSAR-X InSAR coherence. Remote Sens 2018;10:1873.
21. Schepanski K, Wright TJ, Knippertz P. Evidence for flash floods over deserts from loss of coherence in InSAR imagery. J Geophys Res 2012; 117. https://doi.org/10.1029/2012JD017580.
22. Young ME, Bruijn Rde, bin Salim Al-Ismaily A. Exploration of an alluvial aquifer in Oman by time-domain electromagnetic sounding. Hydrogeol J 1998;6:383–93.
23. Hadidi A, Holzbecher E, Molenaar RE. Flood mapping in face of rapid urbanization: a case study of wadi Majraf-Manumah, Muscat, Sultanate of Oman. Urban Water J 2020;17:407–15.
24. Sen Z. Wadi hydrology. Boca Raton, Florida: Crc Press; 2008.
25. Stanger G. The hydrogeology of the Oman Mountains. Milton Keynes: The Open University; 1986.
26. Kwarteng AY, Dorvlo AS, Vijaya Kumar GT. Analysis of a 27-year rainfall data (1977–2003) in the Sultanate of Oman. Intl J Climatology 2009;29: 605–17.
27. Ahmed AT, Askri B. Seawater intrusion impacts on the water quality of the groundwater on the Northwest Coast of Oman. Water Environ Res 2016;88:732–40.
28. Najah A, van der Merwe R, Al Shehhi MR. Review of tropical cyclones impacting the Western Arabian sea and Oman. J Oper Oceanography 2025;18:21–39.
29. Shi T, Xu H. Derivation of tasseled cap transformation coefficients for Sentinel-2 MSI At-Sensor reflectance data. IEEE J Sel Top Appl Earth Observations Remote Sensing 2019;12:4038–48.
30. Böhner J, Seilig T. Spatial prediction of soil attributes using terrain analysis and climate regionalisation. Göttinger Geographische Abhandlungen 2006;115:13–28.
31. Truckenbrodt J, Cremer F, Baris I, Eberle J. pyroSAR – a framework for large-scale SAR satellite data processing. ESA Living Planet Symposium 2019.
32. European Space Agency (ESA). (2022). SNAP (Sentinel Application Platform) version 9.0 [Computer software]. Science Toolbox Exploitation Platform (STEP). https://step.esa.int/main/
33. Friedrich C, Löw J, Otte I, Hill S, Förtsch S, Schwalb-Willmann J, et al. A multi-talented datacube: integrating, processing and presenting big geodata for the agricultural end user: Fokus: Biodiversität fördern durch digitale Landwirtschaft, Friedrich C, editor, et al. Stuttgart: Gesellschaft für Informatik eV; 2024.
34. Ullmann T, Serfas K, Büdel C, Padashi M, Baumhauer R. Data processing, feature extraction, and time-series analysis of Sentinel-1 synthetic aperture radar (SAR) imagery: examples from damghan and Bajestan playa (Iran). Z Geomorphol 2019;62:9–39.
35. Dingle Robertson L, McNairn H, van der Kooij M, Jiao X, Ihuoma S, Joosse P, et al. Monitoring autumn agriculture activities using synthetic aperture radar (SAR) and coherence change detection. Heliyon [Internet] 2023;9:e17322. Available from: https://www.cell.com/heliyon/fulltext/s2405-8440(23)04530-9.
36. Zhao J, Li Y, Matgen P, Pelich R, Hostache R, Wagner W, et al. Urban-aware U-Net for large-scale urban flood mapping using multitemporal Sentinel-1 intensity and interferometric coherence. IEEE Trans Geosci Remote Sensing 2022;60:1–21.
37. Abushandi E, Al Sarihi M, Ibrahim O. Assessing flash flood inundation from an extreme rainfall event: case study: wadi Al Jizzi Oman. AQUA – Water Infrastructure, Ecosystems and Society 2023;72:1770–83.
38. Mett M, Aufleger M. Observation of flashflood-related morphology changes in arid areas with the help of optical satellite data: case study Al-Batinah plain in Oman. In: Geophysical Research Abstracts. EGU General Assembly; 2010:8188 p.
39. Plank S. Rapid damage assessment by means of multi-temporal SAR – a comprehensive review and outlook to Sentinel-1. Remote Sens 2014;6: 4870–906.
40. Wang W, Motagh M, Xia Z, Plank S, Orynbaikyzy A, Zhou C, et al. A framework for automated landslide dating utilizing SAR-derived parameters time-series, an enhanced transformer model, and dynamic thresholding. Int J Appl Earth Obs Geoinf 2024;129:103795.
41. Garg S, Dasgupta A, Motagh M, Martinis S, Selvakumaran S. Unlocking the full potential of Sentinel-1 for flood detection in arid regions. Rem Sens Environ 2024;315:114417.
42. Holzbecher E, Ebeid M, Hadidi A, Agirbas E. Interplay of sediment transport and urbanization in wadi environments. In: Surface Environments and Human Interactions. Singapore: Springer Nature; 2024:139–52 pp.
43. Salim AL Hajri F. Enhancing disaster risk reduction and response: a comparison of the complexities of inter-sectoral coordination in the Omani disaster management system 2010-2020. Bournemouth: Bournemouth University; 2023.